PCCP

On the Choice of Reference Orbitals for Linear-Response Calculations of Solution-Phase K-Edge X-Ray Absorption Spectra

Journal:	*Physical Chemistry Chemical Physics*
Manuscript ID	CP-ART-09-2022-004077.R1
Article Type:	Paper
Date Submitted by the Author:	14-Oct-2022
Complete List of Authors:	Carter-Fenk, Kevin; University of California Berkeley, Chemistry Head-Gordon, Martin; University of California Berkeley, Chemistry; Lawrence Berkeley National Laboratory

Journal Name

ARTICLE TYPE

Cite this: DOI: 00.0000/xxxxxxxxxx

On the Choice of Reference Orbitals for Linear-Response Calculations of Solution-Phase K-Edge X-Ray Absorption Spectra†

Kevin Carter-Fenk,[a,‡] and Martin Head-Gordon,[a,b,§]

Received Date
Accepted Date

DOI: 00.0000/xxxxxxxxxx

The simplest response theory methods for computing vertical excitation spectra in condensed-phase are configuration interaction with single excitations (CIS) and linear-response time-dependent density functional theory (TDDFT) within the Tamm-Dancoff approximation. In applications to X-ray absorption spectroscopy (XAS), methods like CIS and TDDFT that codify only single excitations into the wave function are prone to catastrophic errors in main-edge and post-edge features whose shapes act as a crucial fingerprint in structural analyses of liquids. We show that these errors manifest primarily due to a lack of orbital relaxation in conventional linear-response theories and that core-ionized (n–1-electron) references, like those of electron-affinity TDDFT, can eliminate the errors in the spectral profile, even in the highest-energy parts of the post-edge. Crucially, we find that single excitations atop core-ionized references are sufficient to elucidate liquid-phase XAS spectra with semi-quantitative accuracy, opening the door for methods like electron-affinity CIS/TDDFT to be used as efficient alternatives to higher-order wave function approaches.

1 Introduction

X-ray absorption spectroscopy (XAS) provides impeccable insight into local solvation structure in the vicinity of the chromophore.[1] Soft-XAS has been used as a direct probe of microheterogeneity in aqueous acetonitrile solutions[2] and has revealed the contrasting nature between weak ammonia/water and strong ammonium/water hydrogen bonds.[3,4] X-ray absorption fine-structure (XAFS) spectroscopy was also recently applied to study the hydration structure about ions of all of the first row transition metal elements.[5] As the application of XAS-related methods becomes more ubiquitous, it is increasingly important that theoretical methods meet the challenge of modeling XAS in liquid phase to aid in spectral assignments and to shed light on the atomistic structural details that lead to key spectroscopic signatures.

Time-dependent density functional theory (TDDFT)[6–11] in the linear-response regime is the workhorse for the calculation of electronic excited states in large systems. However, core-excited states are problematic in TDDFT due to an improper description of particle-hole interactions and a lack of orbital relaxation.[12–16] Particle-hole interaction refers to the excited electron interacting with the Coulomb hole left behind in the donor orbital after vertical excitation. This effect is totally absent in pure density functionals and only partially captured by hybrid functionals due to the inexact treatment of exchange in density functional theory (DFT).[17,18] In the context of XAS, orbital relaxation refers to the strong polarizing effect on all orbitals due to removing an electron from a core orbital. This effect is nearly absent in all varieties of linear-response methods that include only singly-excited configurations in a wave function generated from ground-state reference orbitals. While TDDFT has shown some promise in modeling liquid-phase XAS, it has not been intensively studied until recently,[5,19–23] leaving the importance of orbital relaxation and particle-hole interaction errors in the condensed phase yet to be thoroughly assessed.

Despite the complexity of the condensed phase, the methods with the most success in reproducing both the energies and intensities of liquid-phase XAS are wave function approaches such as restricted active-space (RAS)[5] and core-valence-separated equation-of-motion coupled-cluster with single and double excitations (CVS-EOM-CCSD).[24] These approaches have been contrasted with transition-potential density functional theory (TP-DFT)[25–27] and TDDFT, and in both cases the success of wave function theory where DFT failed was attributed to the lack of double excitations in the DFT-based approaches.[28] This hypothesis appears to be bolstered by the fact that perturbative inclusion

[a] *Kenneth S. Pitzer Center for Theoretical Chemistry, Department of Chemistry, University of California, Berkeley, CA 94720, USA.*
[b] *Chemical Sciences Division, Lawrence Berkeley National Laboratory, Berkeley, CA 94720, USA*

† Electronic Supplementary Information (ESI) available: Linear shifts applied to all spectra, histogram spectra, and comparison between full EA-TDDFT and EA-TDDFT within the Tamm-Dancoff approximation. See DOI: 00.0000/00000000.

‡ E-mail: carter-fenk@berkeley.edu
§ E-mail: mhg@cchem.berkeley.edu

of double excitations (*e.g. via* CC2 or CIS(D)) generally fails to reproduce core-level spectra in the condensed phase.[24,29] In addition, it was shown that CVS-EOM-CCSD accurately captures the pre-edge and main-edge features due to the variational inclusion of double excitations in the wave function, thereby encoding orbital relaxation into the resultant spectra.[24] The objective of this work is to probe the effects of orbital relaxation on the spectral profiles of liquid-phase XAS as predicted by wave function-based and DFT-based linear response theories.

While it might appear that double excitations are crucial for accurately modeling liquid-phase XAS, the relative contribution of doubly-excited determinants may be significantly lower for other choices of reference orbitals.[30] In the ground state, the electron correlation energy, E_c, is defined as the difference between the exact energy and a mean-field reference E_0: $E_c = E - E_0$. If there are multiple choices for E_0, then E_c is not uniquely defined and one must be specific (*e.g.* using spin-polarized versus spin-restricted orbitals). Such considerations are even more vital for core excitations, which create a core hole at a specific atomic site, and reattach the electron into an empty valence orbital. One could create an open-shell configuration using ground-state orbitals Φ_0^* with energy $E_0^*(0)$, yielding $E_c^*(0) = E^* - E_0^*(0)$. Or, one could make a much better determinant by minimizing the energy E_0^* of the open-shell configuration, yielding state-specific optimized orbitals $\Phi^*(\text{opt})$ and a much smaller correlation energy $E_c^*(\text{opt}) = E^* - E_0^*(\text{opt})$. The difference $E_c^*(0) - E_c^*(\text{opt})$, which describes the influence of orbital relaxation in the excited state, is 10–15 eV for core excitations in second-row atoms.

State-specific approaches to XAS such as orbital-optimized DFT perform that relaxation explicitly, and with spin adaptation, have been demonstrated to work very well.[31–34] Alternatively, a good approximation is to use the orbitals of the core ion and then reattach the electron, as is done in the static-exchange approximation (STEX) or electron-affinity CIS (EA-CIS).[35–39] Orbitals of the core-ion reference can be further improved by the inclusion of DFT correlation; a feat accomplished by our group's recently proposed electron-affinity TDDFT (EA-TDDFT) approach.[40] None of these approaches explicitly include double (or higher-order) excitations, but because they use site-specific orbital-optimized references more of the correlation energy is recovered in accordance with $E_c^*(0) - E_c^*(\text{opt}) > 0$. In this sense, these methods can be considered to recover "implicit" or "mean-field" correlation effects, whereas methods that use the n-electron ground state reference require "explicit" correlation supplied by direct inclusion of ancillary excitations. Herein, we will explore the importance of implicit correlation as it pertains to solution-phase XAS calculations by choosing the core-ionized orbitals as the initial reference for linear-response theories that incorporate only single excitations into the final wave function.

2 Theory

Electron-affinity methods, which use the core-ion reference, generally supply significant improvements to core excitation energies predicted by linear-response theories such as CIS, TDDFT, equation-of-motion coupled-cluster, and algebraic diagrammatic construction methods.[40–44] In this work, we study the impact of orbital relaxation on liquid-phase XAS by comparison of CIS and TDDFT, which use the ground-state reference, alongside EA-CIS and EA-TDDFT, which use the core-ion reference. This comparison allows a straightforward assessment of the impact of orbital relaxation on the XAS spectral profile because the former two methods encode very little orbital relaxation into the resultant spectrum whereas the latter two approaches have relaxation explicitly built into the reference orbitals.

The EA-TDDFT approach begins by self-consistently optimizing the density of a core-ionized configuration that hosts a core hole in the orbital of interest. The missing electron is then reattached to reform the n-electron system without changing the molecular orbitals (thus preserving the orbital relaxation obtained from the initial optimization). This is followed by a calculation of the n-electron linear response that is corrected for particle-hole self-interaction error by means of an exact first-order elimination of the residual Coulomb interaction with the core hole.[40] The working equations for EA-TDDFT incorporate orbital relaxation and correct particle-hole attraction and take the form,

$$\begin{aligned} A_{ia,ib} &= \tilde{E}^n \delta_{ab} + F_{ab}^+ - \varepsilon_i^+ \delta_{ab} + (ia|ib) + (1 - C_{\text{HF}})(ia|f_{\text{xc}}^+|ib) \\ B_{ia,ib} &= (ia|ib) + (1 - C_{\text{HF}})(ia|f_{\text{xc}}^+|ib) \end{aligned} \tag{1}$$

where $\tilde{E}^n = E^+ + \varepsilon_i^+$ is the nonstationary energy of the n-electron system constructed by reattaching the n^{th}-electron to the self-consistently optimized orbitals of the core ion. The energy of the core-ionized state is E^+, the core-hole orbital i has energy ε_i^+, F_{ab}^+ are elements of the virtual-virtual block of the n–1-electron Fock matrix, $(ia|ib)$ is an exchange integral in Mulliken notation, C_{HF} is the coefficient of exact Hartree-Fock (HF) exchange, and

$$(ia|f_{\text{xc}}^+|ib) = \frac{\partial V_{\text{xc}}[\rho^+(\mathbf{r})]}{\partial \rho^+(\mathbf{r})} \tag{2}$$

is the exchange-correlation kernel computed as a functional of the density of the core-ionized state. All of the above integrals incorporate only the core orbital i in the occupied space (implying core-valence separation)[45–48] and use molecular orbitals that were optimized for the core-ionized state. Within generalized Kohn-Sham theory, these expressions reduce to electron-affinity time-dependent Hartree-Fock (EA-TDHF) in the limit of the HF functional and represent an exact first-order correction to particle-hole interaction errors encountered in TDDFT calculations that employ the adiabatic approximation.[6,40,49,50]

While we could have written Eq. 1 without invoking the orbital energy ε_i, we chose this form to illustrate that EA-TDDFT comes from the sum of two linear responses, the first of which simply modifies the reference energy by ε_i. This form is also useful because it is simple to see that after factoring $\tilde{E}^n \delta_{ab}$ out of the $\mathbf{A}$ matrix, that the matrix $\mathbf{A} - \mathbf{B}$ is positive definite, allowing for the non-Hermitian eigenvalue equation of EA-TDDFT to be solved by transformation into a Hermitian one,[51]

$$(\mathbf{A} - \mathbf{B})^{1/2}(\mathbf{A} + \mathbf{B})(\mathbf{A} - \mathbf{B})^{1/2}\mathbf{Z} = \lambda^2 \mathbf{Z} \tag{3}$$

where $\mathbf{Z} = (\mathbf{A} - \mathbf{B})^{-1/2}(\mathbf{X} + \mathbf{Y})$ and $\mathbf{X}$ and $\mathbf{Y}$ are the excitation and de-excitation amplitudes, respectively. The excitation energies

are then obtained by adding $\tilde{E}^n$ back into the electron-affinities λ and referencing this value back to the self-consistent n-electron ground state energy E^n_{SCF},

$$\omega_p = \tilde{E}^n + \lambda_p - E^n_{\mathrm{SCF}} \,. \tag{4}$$

This summarizes our recent implementation of the full EA-TDDFT equations, but for reasons outlined below we opt for the Tamm-Dancoff approximation (TDA) for K-edge XAS calculations.[18,52–54]

Although the above expressions correspond to the full EA-TDDFT theory, we apply the TDA throughout this work (*i.e.* we set $\mathbf{B} = 0$ in Eq. 1).[54] Our use of the TDA is justified by direct comparison with K-edge spectra of NH_3(aq) computed using the full EA-TDDFT equations in Fig. S1. Despite the fact that the TDA does not abide strictly by the Thomas-Reiche-Kuhn sum rule, the spectral profiles are unchanged and the excitation energies differ by just 0.001 eV. For K-edge spectra, where an electron is excited from a 1s orbital into a valence virtual orbital, this result makes a great deal of sense because the elements of the **B** matrix are proportional to the overlap of the donor and acceptor orbitals. Because the elements of **B** are already nearly zero, the TDA gives results similar to the full EA-TDDFT expressions. Given that the TDA is only a minor approximation in the case of K-edge XAS, we advocate for its use (henceforth implied) within the EA-TDDFT formalism.

Finally, the states obtained with EA-TDDFT are orthogonal amongst themselves but nonorthogonal to the n-electron ground state. Unlike STEX, which accounts for this nonorthogonality by projecting the contributions of the n-electron ground state out of the Hamiltonian,[37–39] the EA-CIS and EA-TDDFT approaches make the approximation that this is only a small correction, ignoring the nonorthogonality in the calculation of the excitation energies. While the excitation energies, computed *via* Eq. 4 are insensitive to this approximation with statistical differences of just ± 0.01 eV between EA-CIS and STEX, the transition dipole moments are far more sensitive to nonorthogonality and must be computed by projecting out the overlap with the ground state,

$$\vec{\mu} = \sum_a X^a_i \left(\langle \Phi_0 | \hat{\mu} | \Psi^a_i \rangle - \langle \Phi_0 | \hat{\mu} | \Phi_0 \rangle \langle \Phi_0 | \Psi^a_i \rangle \right) , \tag{5}$$

where Φ_0 is the n-electron ground state determinant, Φ^a_i are core-excited configurations, and X^a_i are EA-TDDFT excitation amplitudes.

Neither EA-CIS nor EA-TDDFT explicitly encode double excitations into the wave function. Instead, nearly all of the orbital relaxation in the resultant spectra comes from the self-consistent optimization of the core-ionized reference orbitals. In this sense, the only difference between EA-CIS and CIS is the reference state while EA-TDDFT includes an additional correction for particle-hole self-interaction error relative to TDDFT. Any differences in the qualitative nature of the electron-affinity-based spectra and those of standard linear response theories can therefore be attributed to the difference in the reference orbitals (*i.e.* orbital relaxation) in the case of CIS/EA-CIS along with an additional (roughly linear)[13] correction to the excitation energies in the case of TDDFT/EA-TDDFT.

3 Results & Discussion

In this work, we study liquid-phase XAS of water, NH_3(aq), and NH_4^+(aq) as all of these solutions have exceptional chemical relevance. The structure of liquid water has been the focus of some controversy, where the standard tetrahedral coordination was challenged with a purported "rings-and-chains" geometry.[55–57] The NH_3(aq) and NH_4^+(aq) systems play a key role in the nitrogen cycle,[58] and represent prototypical N-containing systems for the study of hydrogen bonding.[3]

We generated 1 ns ($T = 300$ K) trajectories of each of these liquids using classical molecular dynamics driven by the AMOEBA polarizable force field (see Computational Details for simulation information).[59] A total of 50 structures were collected by sampling every 20 ps across the duration of the simulation. To extract clusters for quantum mechanical calculations, the radial pair-distribution function (Fig. 1) was used to inform a radial cutoff that corresponded to the first two hydration shells around the solute molecule.

The average coordination number of liquid water was determined to be 4.7, which is consistent with previous results and with an overall tetrahedral structure.[56] In the case of NH_3, integration to the first minimum of $g_{\mathrm{NO}}(r)$ (Fig. 1b) yields a coordination number of 1.2. This value, along with the overall structureless form of $g_{\mathrm{NO}}(r)$, are consistent with the finding that NH_3 forms one hydrogen bond via its lone pair while freely rotating along its C_{3v} axis.[3] Finally, the coordination number of NH_4^+ is found to be 6.6 due to the fact that it hosts a positive charge, greatly enhancing the polarity of the N–H bonds and leading to a much more structured $g_{\mathrm{NO}}(r)$ (Fig. 1c) that is also consistent with previous results.[3]

The calculated XAS spectra for each system are shown in Fig. 2. It is immediately apparent from Fig. 2a–c that standard CIS and TDDFT are completely inappropriate for the liquid-phase problem, as the spectral profiles are so distorted that assignment of even the pre-edge features becomes impossible. Despite attempts to rigidly shift the calculated spectra, the computed spectral profiles (although consistent with prior work on liquid water)[19] are simply qualitatively incorrect. This problem does not stem from a lack of correlation, as evidenced by the qualitative similarity between CIS and TDDFT results. Even more unsettling is that the TDDFT calculations feature the short-range corrected SRC1-R1 functional,[61–63] which is parameterized specifically for XAS by means of a cancellation between particle-hole self-interaction errors (*i.e.* errors in the potential due to the DFT *ansatz*) and orbital relaxation error.[40] Instead of a lack of correlation (in the case of CIS) or errors in the DFT potential, it would appear that the large errors exhibited by CIS and TDDFT likely emerge from the choice of the n-electron (ground state) reference determinant. This choice leads to large errors in the spectral profiles predicted by CIS and TDDFT because it precludes an adequate description of orbital relaxation in any spectrum comprised entirely of single excitations.

In stark contrast, the results obtained with EA-CIS and EA-TDDFT (Fig.2d–f) capture the pre-edge, main-edge, and post-

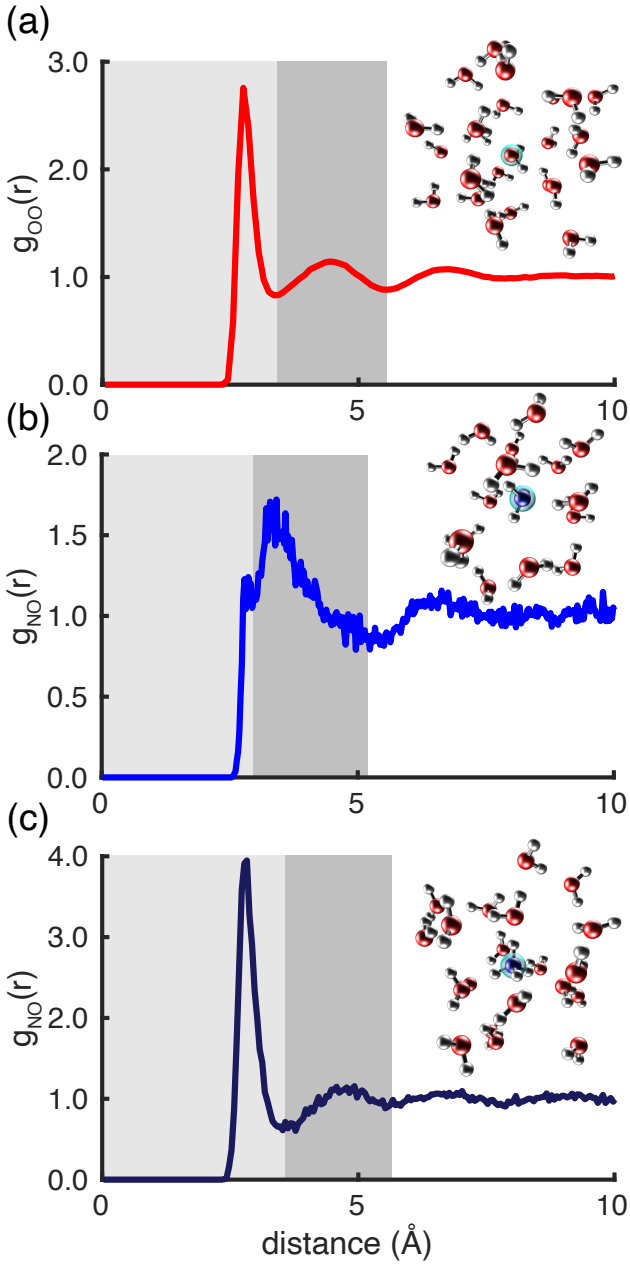

Fig. 1 XO radial pair-distribution functions for the systems studied in this work, where X is the (a) O of H_2O, (b) N of NH_3, and (c) N of NH_4^+. The light gray bar shows the integration bounds used to compute the coordination number and the light gray plus dark gray bars indicate the bounds applied to extract two hydration shells from each snapshot. Representative structures selected under this criterion are shown as insets and the 1s orbital of interest is displayed on the relevant atom.

edge features with high fidelity. Interestingly, the rigid shift of the EA-TDDFT spectra that was chosen to align the pre-edge features to experiment (shift values in Tab. S1) is of similar magnitude to the shift that was required to align CVS-EOM-CCSD results for NH_3 and NH_4^+ with experiment (about -2 eV).[24] This suggests that the peak positions of EA-TDDFT are of similar quality to those predicted by CVS-EOM-CCSD and that EA-TDDFT still shows a remarkable improvement over methods like damped TDDFT (with a similar functional) which requires a shift of 15 eV for the O K-edge of liquid water.[20] The magnitude of the shift is, of course, functional specific and may be reduced with different choices of density functional *ansatz*, such as functionals that are parameterized to recover Koopman's-like ionization potentials or electron affinities,[64] but this avenue of research is left for future work. Nonetheless, the improvements in both peak position and peak intensity supplied by EA-TDDFT/EA-CIS relative to TDDFT/CIS suggest that orbital relaxation is the primary source of error in linear-response-based XAS calculations, and that merely changing the initial reference from that of the n-electron ground state to the core-ionized n–1-electron determinant is sufficient to recover the entire spectrum without ever explicitly including double (or higher) excitations. The good agreement of EA-TDDFT with CVS-EOM-CCSD also implies that orbital relaxation is indeed the primary role of double excitations in the core-excitation spectra of solvated chromophores.

Overall, the EA-CIS spectra are qualitatively similar to those predicted by EA-TDDFT, with the exception that an additional curiosity emerges in the spectrum of liquid water (Fig. 2f). Whereas EA-TDDFT predicts that the main-edge peak at $\sim$ 538 eV is the most intense, followed by a small shoulder at $\sim$ 539 eV and then a sizable post-edge peak at $\sim$ 542 eV, the EA-CIS spectrum injects most of the intensity into the post-edge feature, leaving the main-edge peak to be the second-lowest in intensity. This qualitative failure of EA-CIS emerges from a lack of explicit correlation effects in the core-ionized reference orbitals, and is likely a result of spectral compression such that higher-energy features are blending in with the highest-energy peak in the post-edge.[65] Interestingly, liquid water is the only spectrum that contains such qualitative differences, but it is clear from Fig. 2d–f that EA-CIS does exaggerate the intensities of high-energy features relative to EA-TDDFT and that the features do appear to be compressed relative to their counterparts in EA-TDDFT. Clearly orbital relaxation plays a more sizable role in the overall shape of a given spectrum, but correlation (or lack thereof) can also play a significant qualitative role in the spectral profile. In order to ensure that these arguments were not crafted atop the assumption of a Gaussian line shape, we have reproduced these conclusions by replotting each spectrum using weighted histograms (Fig. S2) which forego any assumption about the spectral distribution.

With respect to liquid water in particular, our molecular dynamics simulations suggest a tetrahedral framework and the EA-TDDFT XAS calculations are in excellent agreement with experiment. The ionization potential of the core 1s orbital (Fig. 2) is also within 0.5 eV of experimental photoelectron measurements.[66] Interestingly, we find that EA-TDDFT also predicts a small shoulder feature at $\sim$ 544 eV that was previously identified using damped TDDFT.[20] The same feature is amplified in the EA-CIS spectrum due to spectral compression, appearing as a fifth peak rather than a smaller shoulder. Although this feature is measurable in ice,[20] the split post-edge peak in liquid water remains to be validated by experimental evidence. The amplification of the post-edge features in theoretical calculations might indicate that the water structure supplied by the molecular dynamics (in our case, driven by the AMOEBA force field) is slightly too ice-like.[67] Nonetheless, it is interesting to note that multiple theo-

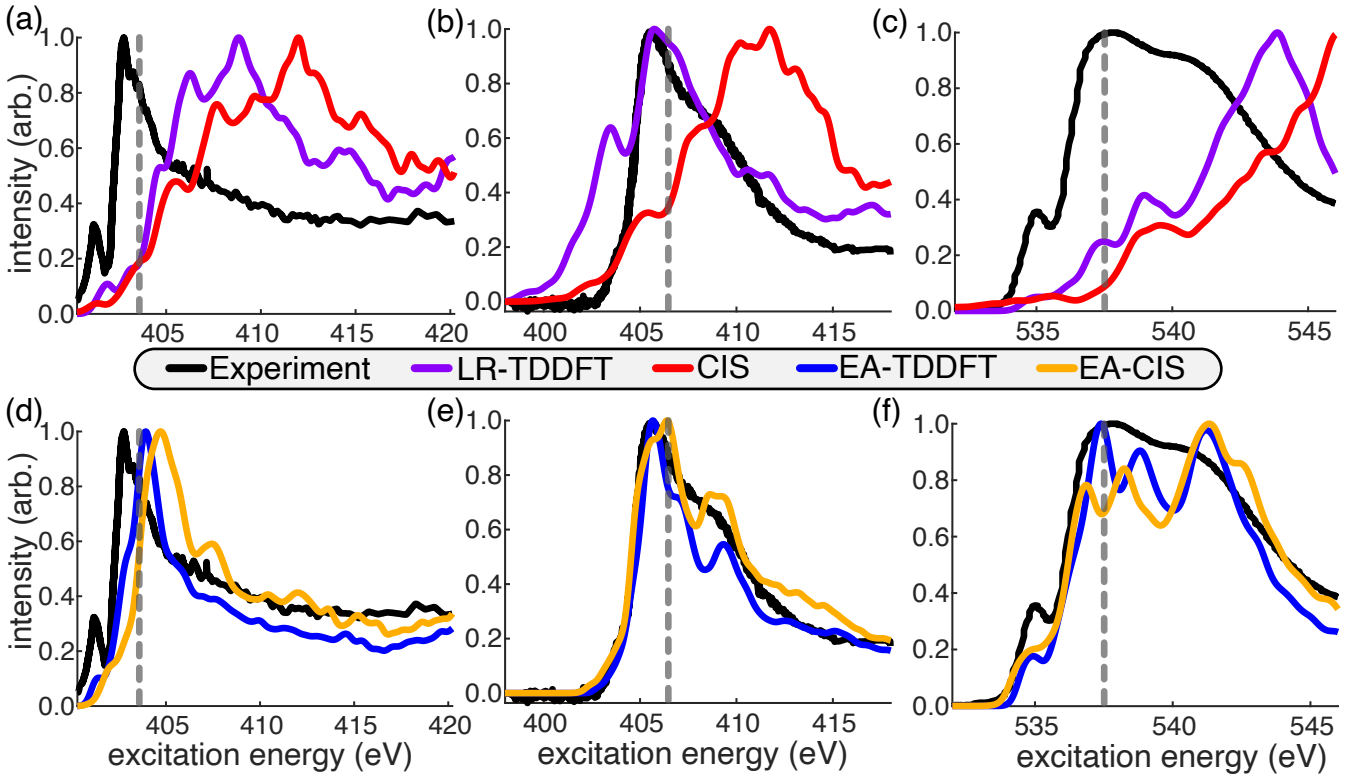

Fig. 2 Calculated XAS profiles using standard linear-response methods (LR-TDDFT/CIS) for (a) NH_3(aq), (b) NH_4^+(aq) and (c) liquid water along with XAS profiles using orbital-optimized linear-response methods (EA-TDDFT/EA-CIS) for (d) NH_3(aq), (e) NH_4^+(aq), and (f) liquid water. Each spectrum is an average over 50 snapshots from a molecular dynamics trajectory. When possible, spectra were shifted to align the pre-edge feature with experiment (details in Tab. S1). The dashed gray lines indicate the rCAM-B3LYP/aug-pcX-2 ionization potential, calculated *via* ΔSCF. Experimental spectra for NH_3(aq) and NH_4^+(aq) were reproduced from Ref. 3 and liquid water data are taken from Ref. 60.

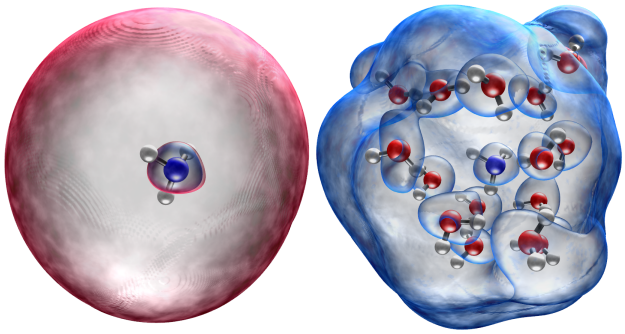

Fig. 3 Example of the "frustrated" Rydberg concept. States that comprise the pre-edge feature in NH_3 have 3s Rydberg-like character (left), but nearby water molecules distort the symmetry (right). Both isosurfaces represent a volume containing 60% of the electron probability amplitude.

retical approaches have implied the existence of the additional post-edge peak.

In terms of spectral assignments, the pre-edge feature in all of these spectra takes the form of a "frustrated" Rydberg-like excitation (Fig. 3), which is a solution-phase analog of 1s→3s transitions where the symmetry of the final state is perturbed by the presence of the solvent molecules. This distorted symmetry results in weak pre-edge features that would otherwise be symmetry forbidden. Of course, in our limited two-hydration-shell models, we do not completely capture the degree of orbital distortion that might be otherwise caused by an infinite system, so we refer to this state as "Rydberg-like" as opposed to a true frustrated Rydberg excitation. The main-edge features are much more delocalized, and the post-edge transitions are all unbound (exceeding the ionization potential of the solute) excitations into high-energy orbitals that might be characterized as continuum states.

Previous work, along with the electron-affinity methods discussed here, has established that the pre-edge and main-edge features may only be accurately captured if variational orbital relaxation is encoded into the wave function.[24] However, it was also suggested that a lack of double excitations (primarily functioning as a source of orbital relaxation) was also to blame for the failure of TP-DFT to capture the long post-edge tail exhibited by NH_3 and NH_4^+. We investigate the origin of the post-edge tail in NH_3 and NH_4^+ by replicating the size of the explicit quantum mechanical solvent subsystem (four coordinating water molecules) from Ref. 24 and computing the full spectrum using EA-TDDFT.

The EA-TDDFT spectra in Fig. 4 show the same qualitative features as those calculated using CVS-EOM-CCSD, including the significant drop in intensity in the range 406–411 eV for $NH_3 \cdot (H_2O)_4$ and 409–414 eV for $NH_4^+ \cdot (H_2O)_4$. While the CVS-EOM-CCSD calculations were truncated at 30 roots, the EA-TDDFT calculations were not truncated, suggesting that this decline in intensity is a true feature of the four-explicit-water spectrum. Overall, the fea-

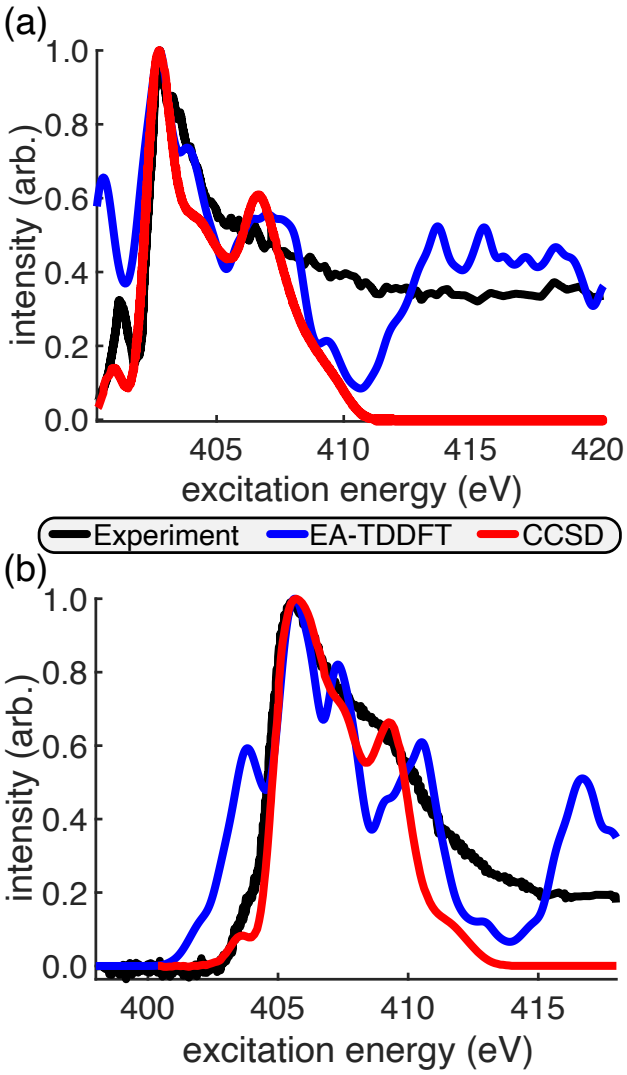

Fig. 4 Spectra with only four explicit quantum-mechanical water molecules for (a) NH_3 and (b) NH_4^+ embedded within a molecular-mechanics-based polarizable embedding model (CVS-EOM-CCSD) or a polarizable continuum model (EA-TDDFT). The CVS-EOM-CCSD spectra are from Ref. 24. For direct comparison, each spectrum was rigidly shifted such that the highest-intensity features overlap with the experimental spectrum.

tures of the post-edge are not adequately captured by EA-TDDFT or CVS-EOM-CCSD if only four explicit water molecules are used, but the spectra in Fig. 2 that contain two hydration shells clearly approximate the bulk spectrum very closely. The EA-TDDFT results also overemphasize some of the pre-edge features in both spectra relative to CVS-EOM-CCSD, which in itself is undesirable. Failure of both EA-TDDFT and CVS-EOM-CCSD in the post-edge region implies that the four-water model is simply too small to reliably predict solution-phase XAS, pointing towards the interesting conclusion that the long post-edge tails in NH_3 and NH_4^+ are a result of many-water cooperativity. It is sensible that the post-edge tails depend on many explicit water molecules because the orbitals that contribute to excitations in this high-energy regime are extremely delocalized. Without a sizable number of explicit water molecules, the model cannot accurately describe the extended nature of the excited states that comprise the post-edge tail. The role of the choice of basis set (atom-centered versus plane-wave) on the post-edge features is an interesting avenue for future work.

The small post-edge tail obtained *via* TP-DFT[24] likely stems from a combination of too-few explicit water molecules, the use of a single set of molecular orbitals to describe both ground and excited states, and that the Koopman's-like description of the excitation energies is inadequate. While TP-DFT and other transition potential methods based on coupled cluster theory[68,69] include implicit electron correlation through a mean-field description of orbital relaxation effects much like EA-TDDFT, the adherence of transition potential methods to a single set of molecular orbitals requires some degree of error cancellation between the ground and excited states in order to attain reasonable accuracy. Unlike TP-DFT, which uses Koopman's-like orbital energy differences to calculate the vertical excitation energies from a single set of orbitals, EA-TDDFT uses the core-ion orbitals to describe the excited states while the self-consistently optimized ground state orbitals are used for the ground state when calculating excitation energies (Eq. 4). By virtue of using two sets of orbitals, EA-TDDFT is capable of describing the ground state and excited states with the best orbitals for each case. EA-TDDFT is also a formally exact linear-response theory, so its description of excited states takes the form of a linear combination of singly-excited determinants, which is likely a better description of delocalized continuum states than that of TP-DFT. Finally, we have shown that the four-water model is insufficient for capturing the features of the post-edge, even at the level of CVS-EOM-CCSD, so the abrupt decline in the intensity of the post-edge should be expected even if TP-DFT performs well in these systems.

In the case of our two-hydration shell EA-TDDFT calculations, where the post-edge features are adequately recovered, we can draw some conclusions regarding the connection between the spectral profiles and the hydration structure at both small and large distances from the chromophore. For instance, the post-edge tail in the NH_3(aq) spectrum has fewer features than those of water or NH_4^+(aq) and we have just established that it depends on continuum states that require many explicit water molecules to resolve. We attribute the long post-edge tail to the free rotation of NH_3 about the C_{3v} axis and correlate it to the structureless region at and beyond the second hydration shell (> 5 Å) in the NH_3(aq) radial distribution function (Fig. 1b). The more structured hydration behavior of water and NH_4^+(aq) result in post-edge tails that host more features, including a split post-edge peak in the case of water. Along the same vein, the results with only four explicit water molecules allow us to confidently assign the pre-edge and main-edge features to the immediately coordinating water molecules within the first hydration shell. In the case of ammonia, this means that the pre- and main-edge peaks are dominated by the coordination of NH_3 to just one water molecule, suggesting that these features can be reliably used as a direct probe of H-bonding in NH_3(aq).

4 Conclusion

In this work, we have demonstrated through the use of EA-CIS and EA-TDDFT that linear-response approaches are completely adequate for the description of liquid-phase XAS if orbital relaxation is taken into account at the level of the reference state. Contrastingly, standard linear-response approaches that use the *n*-electron ground state reference are entirely inappropriate for application to the condensed phase and should be avoided, even in calculations of the pre-edge. This finding is cohesive with the idea that the influence of double excitations on a spectrum can be limited largely to supplying additional orbital relaxation that is missing in the standard *n*-electron ground state reference determinant.[30] Furthermore, the choice of a core-ion reference supplies implicit correlation effects at the mean-field level, permitting an accurate description of liquid-phase XAS spectral profiles at the level of single excitations. While we did not perform algebraic diagrammatic construction (ADC) calculations in this work, it is worth noting that we expect our conclusions to be general. Similar improvements should be expected in solution-phase XAS for approaches that include perturbative electron correlation (*i.e.* CC2 or ADC) effects atop core-ion reference orbitals,[43,44] but we leave intensive study of this hypothesis for future work.

Computational Details

The classical molecular dynamics calculations were carried out using Tinker v8.1.[70] Each 14.27 Å^3 simulation cell contained 96 solvent H_2O molecules and one solute molecule (H_2O, NH_3, or NH_4^+) that was constrained to remain at the center of the cell throughout the dynamics. The geometries were optimized at 0 K before a 10 ps ($\Delta t = 1$ fs) simulation to heat the system up to 300 K using the Nosé-Hoover thermostat within the NVT ensemble.[71,72] Production runs were then carried out for 1 ns under these same conditions. All quantum chemistry calculations were performed with a development version of the Q-Chem 5.4 software package.[73] Density functional calculations utilized a dense grid containing 99 radial points treated under the Euler-Maclaurin scheme[74] and 590 angular points using a Lebedev quadrature[75,76] for the evaluation of the exchange-correlation potential. All DFT calculations employ the exact two-component X2C Hamiltonian to self-consistently account for scalar relativistic effects.[34,77–84] The EA-TDDFT calculations used the rCAM-B3LYP functional,[85] which has been established to perform well for XAS,[40] whereas standard TDDFT calculations employed the SRC1-R1 functional that was specifically optimized for XAS with TDDFT. A mixed basis set was employed in all calculations using aug-pcX-2[86] for the central solute atom, pcseg-1[87] for all H atoms, and the doubly-augmented d-aug-pcseg-1 basis set for all solvent O atoms. Double-augmentation of aug-pcseg-1 was obtained through a simple geometric sequence protocol.[88] All XAS calculations on the solute+four-water model and the solute+two-hydration shell model are performed using a conductor-like polarizable continuum model[89,90] with a solvent accessible surface (probe radius = 1.4 Å)[91] in order to capture the long-range electrostatic effect of the aqueous environment without allowing dielectric to intercalate between explicit solvent/solute molecules. The XAS calculations on systems with two hydration shells of explicit water molecules included an average of 16, 23, and 24 water molecules for NH_3(aq), NH_4^+(aq), and liquid water, respectively. All computed spectra were broadened to obtain a full-width at half-maximum of 0.4 eV in accordance with Ref. 24.

Conflicts of Interest

The authors have no conflicts of interest to declare.

Acknowledgements

This work was supported by the Director, Office of Science, Office of Basic Energy Sciences, of the U.S. Department of Energy under Contract No. DE-AC02-05CH11231. K. C.-F. would like to thank Juan Arias-Martinez and Leonardo Cunha for fruitful discussions.

Notes and references

1 Y. Joly and S. Grenier, John Wiley & Sons, Ltd., West Sussex, 2016.

2 M. Nagasaka, H. Yuzawa, and N. Kosugi, Microheterogeneity in aqueous acetonitrile solution probed by soft x-ray absorption spectroscopy, *J. Phys. Chem. B*, 2020, **124**, 1259–1265.

3 M. Ekimova, W. Quevedo, Ł. Szyc, M. Iannuzzi, P. Wernet, M. Odelius, and E. T. J. Nibbering, Aqueous Solvation of Ammonia and Ammonium: Probing Hydrogen Bond Motifs with FT-IR and Soft X-ray Spectroscopy, *J. Am. Chem. Soc.*, 2017, **139**, 12773–12783.

4 M. Ekimova, M. Kubin, M. Ochmann, J. Ludwig, N. Huse, P. Wernet, M. Odelius, and E. T. J. Nibbering, Soft X-ray Spectroscopy of the Amine Group: Hydrogen Bond Motifs in Alkylamine/Alkylammonium Acid–Base Pairs, *J. Phys. Chem. B*, 2018, **122**, 7737–7746.

5 S. Ghosh, H. Agarwal, M. Galib, B. Tran, M. Balasubramanian, N. Singh, J. L. Fulton, and N. Govind, Near-Quantitative Predictions of the First-Shell Coordination Structure of Hydrated First-Row Transition Metal Ions Using K-Edge X-ray Absorption Near-Edge Spectroscopy, *J. Phys. Chem. Lett.*, 2022, **13**, 6323–6330.

6 M. E. Casida, Time-dependent density functional response theory for molecules, in *Recent Advances in Density Functional Methods, Part I*, ed. D. P. Chong, Vol. I of *Recent Advances in Computational Chemistry;* World Scientific, River Edge, NJ, 1995; chapter 5, pp. 155–192.

7 M. Petersilka, U. J. Gossmann, and E. K. U. Gross, Excitation energies from time-dependent density-functional theory, *Phys. Rev. Lett.*, 1996, **76**, 1212–1215.

8 R. Bauernschmitt and R. Ahlrichs, Treatment of electronic excitations within the adiabatic approximation of time dependent density functional theory, *Chem. Phys. Lett.*, 1996, **256**, 454–464.

9 F. Furche, On the density matrix based approach to time-dependent density functional response theory, *J. Chem. Phys.*, 2001, **114**, 5982–5992.

10 M. A. L. Marques and E. K. U. Gross, Time-dependent density functional theory, *Annu. Rev. Phys. Chem.*, 2004, **55**, 427–455.

11 ed. M. A. L. Marques, N. T. Maitra, F. M. S. Nogueira, E. K. U.

Gross, and A. Rubio, Vol. 837 of *Lecture Notes in Physics*, Springer, New York, 2012.

12 P. J. Lestrange, P. D. Nguyen, and X. Li, Calibration of energy-specific TDDFT for modeling K-edge XAS spectra of light elements, *J. Chem. Theory Comput.*, 2015, **11**, 2994–2999.

13 A. Chantzis, J. K. Kowalska, D. Maganas, S. DeBeer, and F. Neese, *Ab initio* wave function-based determination of element specific shifts for the efficient calculation of x-ray absorption spectra of main group elements and first row transition metals, *J. Chem. Theory Comput.*, 2018, **14**, 3686–3702.

14 C. D. Rankine and T. J. Penfold, Progress in the theory of x-ray spectroscopy: From quantum chemistry to machine learning and ultrafast dynamics, *J. Phys. Chem. A*, 2021, **125**, 4276–4293.

15 A. Bussy and J. Hutter, First-principles correction scheme for linear-response time-dependent density functional theory calculations of core electronic states, *J. Chem. Phys.*, 2021, **155**, 034108:1–10.

16 A. Bussy and J. Hutter, Efficient and low-scaling linear-response time-dependent density functional theory implementation for core-level spectroscopy of large and periodic systems, *Phys. Chem. Chem. Phys.*, 2021, **23**, 4736–4746.

17 A. Dreuw and M. Head-Gordon, Failure of time-dependent density functional theory for long-range charge-transfer excited-states: The zincbacteriochlorin–bacteriochlorin and bacteriochlorophyll–spheroidene complexes, *J. Am. Chem. Soc.*, 2004, **126**, 4007–4016.

18 A. Dreuw and M. Head-Gordon, Single-reference ab initio methods for the calculation of excited states of large molecules, *Chem. Rev.*, 2005, **105**, 4009–4037.

19 G. Brancato, N. Rega, and V. Barone, Accurate density functional calculations of near-edge x-ray and optical absorption spectra of liquid water using nonperiodic boundary conditions: The role of self-interaction and long-range effects, *Phys. Rev. Lett.*, 2008, **100**, 107401:1–4.

20 T. Fransson, I. Zhotobriukh, S. Coriani, K. T. Wikfeldt, P. Norman, and L. G. M. Pettersson, Requirements of first-principles calculations of x-ray absorption spectra of liquid water, *Phys. Chem. Chem. Phys.*, 2016, **18**, 566–583.

21 T. F. Stetina, A. E. Clark, and X. Li, X-ray absorption signatures of hydrogen-bond structure in water–alcohol solutions, *Int. J. Quantum Chem.*, 2018, **119**, e25802:1–6.

22 A. Wildman, E. Martinez-Baez, J. Fulton, G. Schenter, C. Pearce, A. E. Clark, and X. Li, Anticorrelated contributions to pre-edge features of aluminate near-edge x-ray absorption spectroscopy in concentrated electrolytes, *J. Phys. Chem. Lett.*, 2018, pp. 2444–2449.

23 N. A. Phillips, P. W. Smith, T. D. Tilley, and S. G. Minasian, Gauging aromatic conjugation and charge delocalization in the aryl silanes PhnSiH4-n (n = 0–4), with silicon K-edge XAS and TDDFT, *Dalton Trans.*, 2020, **49**, 13176–13184.

24 P. Reinholdt, M. L. Vidal, J. Kongsted, M. Iannuzzi, S. Coriani, and M. Odelius, Nitrogen K-Edge X-ray Absorption Spectra of Ammonium and Ammonia in Water Solution: Assessing the Performance of Polarizable Embedding Coupled Cluster Methods, *J. Phys. Chem. Lett.*, 2021, **12**, 8865–8871.

25 J. C. Slater, Statistical exchange-correlation in the self-consistent field, *Adv. Quantum Chem.*, 1972, **6**, 1–92.

26 A. R. Williams, R. A. deGroot, and C. B. Sommers, Generalization of Slater's transition state concept, *J. Chem. Phys.*, 1975, **63**, 628–631.

27 K. Hirao, T. Nakajima, and B. Chan, An improved Slater's transition state approximation, *J. Chem. Phys.*, 2021, **155**, 034101:1–9.

28 B. G. Levine, C. Ko, J. Quenneville, and T. J. Martínez, Conical intersections and double excitations in time-dependent density functional theory, *Mol. Phys.*, 2006, **104**, 1039–1051.

29 A. Sadybekov and A. I. Krylov, Coupled-cluster based approach for core-level states in condensed phase: Theory and application to different protonated forms of aqueous glycine, *J. Chem. Phys.*, 2017, **147**, 014107:1–11.

30 G. M. J. Barca, A. T. B. Gilbert, and P. M. W. Gill, Excitation number: Characterizing multiply excited states, *J. Chem. Theory Comput.*, 2018, **14**, 9–13.

31 D. Hait and M. Head-Gordon, Highly accurate prediction of core spectra of molecules at density functional theory cost: Attaining sub-electronvolt error from a restricted open-shell Kohn–Sham approach, *J. Phys. Chem. Lett.*, 2020, **11**, 775–786.

32 D. Hait and M. Head-Gordon, Orbital optimized density functional theory for electronic excited states, *J. Phys. Chem. Lett.*, 2021, **12**, 4517–4529.

33 K. Carter-Fenk and J. M. Herbert, State-targeted energy projection: A simple and robust approach to orbital relaxation of non-Aufbau self-consistent field solutions, *J. Chem. Theory Comput.*, 2020, **16**, 5067–5082.

34 L. A. Cunha, D. Hait, R. Kang, Y. Mao, and M. Head-Gordon, Relativistic orbital-optimized density functional theory for accurate core-level spectroscopy, *J. Phys. Chem. Lett.*, 2022, **13**, 3438–3449.

35 H. Ågren, V. Carravetta, O. Vahtras, and L. G. M. Pettersson, Direct, atomic orbital, static exchange calculations of photoabsorption spectra of large molecules and clusters, *Chem. Phys. Lett.*, 1994, **222**, 75–81.

36 H. Ågren, V. Carravetta, O. Vahtras, and L. G. M. Pettersson, Direct SCF direct static-exchange calculations of electronic spectra, *Theor. Chem. Acc.*, 1997, **97**, 14–40.

37 K. J. Oosterbaan, A. F. White, and M. Head-Gordon, Non-orthogonal configuration interaction with single substitutions for the calculation of core-excited states, *J. Chem. Phys.*, 2018, **149**, 044116:1–7, Erratum: *ibid*. **149**, 139901:1–2 (2018).

38 K. J. Oosterbaan, A. F. White, and M. Head-Gordon, Non-orthogonal configuration interaction with single subsitutions for core-excited states: An extension to doublet radicals, *J. Chem. Theory Comput.*, 2019, **15**, 2966–2973.

39 K. J. Oosterbaan, A. F. White, D. Hait, and M. Head-Gordon, Generalized single excitation configuration interaction: An investigation into the impact of the inclusion of non-orthogonality on the calculation of core-excited states, *Phys.*

Chem. Chem. Phys., 2020, **22**, 8182–8192.

40 K. Carter-Fenk, L. A. Cunha, J. E. Arias-Martinez, and M. Head-Gordon, *J. Phys. Chem. Lett.*, 2022, **13**, 9664–9672.

41 M. Nooijen and R. J. Bartlett, Equation of motion coupled cluster method for electron attachment, *J. Chem. Phys.*, 1995, **102**, 3629–3647.

42 M. Nooijen and R. J. Bartlett, Description of core-excitation spectra by the open-shell electron-attachment equation-of-motion coupled cluster method, *J. Chem. Phys.*, 1995, **102**, 6735–6756.

43 T. Fransson and A. Dreuw, Simulating x-ray emission spectroscopy with algebraic diagrammatic construction schemes for the polarization propagator, *J. Chem. Theory Comput.*, 2019, **15**, 546–556.

44 A. Dreuw and T. Fransson, Using core-hole reference states for calculating x-ray photoelectron and emission spectra, *Phys. Chem. Chem. Phys.*, 2022, **24**, 11259–11267.

45 L. S. Cederbaum, W. Domcke, and J. Schirmer, Many-body theory of core holes, *Phys. Rev. A*, 1980, **22**, 206–222.

46 A. Barth and L. S. Cederbaum, Many-body theory of core-valence excitations, *Phys. Rev. A*, 1981, **23**, 1038–1061.

47 M. L. Vidal, X. Feng, E. Epifanovsky, A. I. Krylov, and S. Coriani, New and efficient equation-of-motion coupled-cluster framework for core-excited and core-ionized states, *J. Chem. Theory Comput.*, 2019, **15**, 3117–3133.

48 M. F. Herbst and T. Fransson, Quantifying the error of the core–valence separation approximation, *J. Chem. Phys.*, 2020, **153**, 054114:1–11.

49 M. E. Casida and M. Huix-Rotllant, Progress in time-dependent density-functional theory, *Annu. Rev. Phys. Chem.*, 2012, **63**, 287–323.

50 K. Burke, J. Werschnik, and E. K. U. Gross, Time-dependent density functional theory: Past, present, and future, *J. Chem. Phys.*, 2005, **123**, 062206:1–9.

51 R. E. Stratmann, G. E. Scuseria, and M. J. Frisch, An efficient implementation of time-dependent density-functional theory for the calculation of excitation energies of large molecules, *J. Chem. Phys.*, 1998, **109**, 8218–8224.

52 J. E. Del Bene, R. Ditchfield, and J. A. Pople, Self-consistent molecular orbital methods. X. Molecular orbital studies of excited states with minimal and extended basis sets, *J. Chem. Phys.*, 1971, **55**, 2236–2241.

53 J. B. Foresman, M. Head-Gordon, J. A. Pople, and M. J. Frisch, Toward a systematic molecular orbital theory for excited states, *J. Phys. Chem.*, 1992, **96**, 135–149.

54 S. Hirata and M. Head-Gordon, Time-dependent density functional theory within the Tamm-Dancoff approximation, *Chem. Phys. Lett.*, 1999, **314**, 291–299.

55 P. Wernet, D. Nordlund, U. Bergmann, M. Cavalleri, M. Odelius, H. Ogasawara, L. Näslund, T. K. Hirsch, L. Ojamäe, P. Glatzel, et al., The structure of the first coordination shell in liquid water, *Science*, 2004, **304**, 995–999.

56 T. Head-Gordon and M. E. Johnson, Tetrahedral structure or chains for liquid water, *Proc. Natl. Acad. Sci. USA*, 2006, **103**, 7973–7977.

57 F. Tang, Z. Li, C. Zhang, S. G. Louie, R. Car, D. Y. Qiu, and X. Wu, Many-body effects in the X-ray absorption spectra of liquid water, *Proc. Natl. Acad. Sci. USA*, 2022, **119**, e2201258119:1–7.

58 J. N. Galloway, A. R. Townsend, J. W. Erisman, M. Bekunda, Z. Cai, J. R. Freney, L. A. Martinelli, S. P. Seitzinger, and M. A. Sutton, Transformation of the nitrogen cycle: Recent trends, questions, and potential solutions, *Science*, 2008, **320**, 889–892.

59 J. W. Ponder, C. Wu, P. Ren, V. S. Pande, J. D. Chodera, M. J. Schnieders, I. Haque, D. L. Mobley, D. S. Lambrecht, R. A. DiStasio, Jr., M. Head-Gordon, G. N. I. Clark, M. E. Johnson, and T. Head-Gordon, Current status of the AMOEBA polarizable force field, *J. Phys. Chem. B*, 2010, **114**, 2549–2564.

60 J. Meibohm, S. Schreck, and P. Wernet, Temperature dependent soft x-ray absorption spectroscopy of liquids, *Rev. Sci. Instrum.*, 2014, **85**, 103102.

61 N. A. Besley, M. J. G. Peach, and D. J. Tozer, Time-dependent density functional theory calculations of near-edge x-ray absorption fine structure with short-range corrected functionals, *Phys. Chem. Chem. Phys.*, 2009, **11**, 10350–10358.

62 N. A. Besley, Density functional theory based methods for the calculation of x-ray spectroscopy, *Acc. Chem. Res.*, 2020, **53**, 1306–1315.

63 N. A. Besley, Modeling of the spectroscopy of core electrons with density functional theory, *WIREs Comput. Mol. Sci.*, 2021, **12**, e1527:1–22.

64 P. Verma and R. J. Bartlett, Increasing the applicability of DFT. IV. Consequences of ionization-potential improved exchange-correlation potentials, *J. Chem. Phys.*, 2014, **140**, 18A534:1–11.

65 P. Norman and A. Dreuw, Simulating x-ray spectroscopies and calculating core-excited states of molecules, *Chem. Rev.*, 2018, **118**, 7208–7248.

66 K. Nishizawa, N. Kurahashi, K. Sekiguchi, T. Mizuno, and Y. Ogi, High-resolution soft x-ray photoelectron spectroscopy of liquid water, *Phys. Chem. Chem. Phys.*, 2011, **13**, 413–417.

67 J. A. Sellberg, S. Kaya, V. H. Segtnan, C. Chen, T. Tyliszczak, H. Ogasawara, D. Nordlund, L. G. M. Pettersson, and A. Nilsson, Comparison of x-ray absorption spectra between water and ice: New ice data with low pre-edge absorption cross-section, *J. Chem. Phys.*, 2014, **141**, 034507:1–12.

68 M. Simons and D. A. Matthews, Transition-potential coupled cluster, *J. Chem. Phys.*, 2021, **154**, 014106:1–9.

69 M. Simons and D. A. Matthews, Transition-potential coupled cluster II: Optimisation of the core orbital occupation number, *J. Math. Phys.*, 2022, pp. e2088421:1–9.

70 M. Harger, D. Li, Z. Wang, K. Dalby, L. Lagardère, J.-P. Piquemal, J. Ponder, and P. Ren, Tinker-OpenMM: Absolute and relative alchemical free energies using AMOEBA on GPUs, *J. Comput. Chem.*, 2017, **38**, 2047–2055.

71 S. Nose, A unified formulation of the constant temperature molecular dynamics method, *J. Chem. Phys.*, 1984, **81**, 511–519.

72 W. G. Hoover, Canonical dynamics: Equilibrium phase-space distributions, *Phys. Rev. A*, 1985, **31**, 1695–1697.

73 E. Epifanovsky *et al.*, Software for the frontiers of quantum chemistry: An overview of developments in the Q-Chem 5 package, *J. Chem. Phys.*, 2021, **155**, 084801:1–59.

74 C. W. Murray, N. C. Handy, and G. J. Laming, Quadrature schemes for integrals of density functional theory, *Mol. Phys.*, 1993, **78**, 997–1014.

75 V. I. Lebedev, Values of the nodes and weights of ninth to seventeenth order gauss-markov quadrature formulae invariant under the octahedron group with inversion, *USSR Comput. Math. & Math. Phys.*, 1975, **15**, 44–51.

76 V. I. Lebedev, Quadratures on a sphere, *USSR Comput. Math. & Math. Phys.*, 1976, **16**, 10–24.

77 P. Verma, W. D. Derricotte, and F. A. Evangelista, Predicting near edge x-ray absorption spectra with the spin-free exact-two-component Hamiltonian and orthogonality constrained density functional theory, *J. Chem. Theory Comput.*, 2016, **12**, 144–156.

78 K. G. Dyall, Interfacing relativistic and nonrelativistic methods. I. Normalized elimination of the small component in the modified Dirac equation, *J. Chem. Phys.*, 1997, **106**, 9618–9626.

79 W. Kutzelnigg and W. Liu, Quasirelativistic theory equivalent to fully relativistic theory, *J. Chem. Phys.*, 2005, **123**, 241102.

80 M. Iliaš and T. Saue, An infinite-order two-component relativistic Hamiltonian by a simple one-step transformation, *J. Chem. Phys.*, 2007, **126**, 064102.

81 W. Liu and D. Peng, Exact two-component Hamiltonians revisited, *J. Chem. Phys.*, 2009, **131**, 031104.

82 T. Saue, Relativistic Hamiltonians for Chemistry: A Primer, *ChemPhysChem*, 2011, **12**, 3077–3094.

83 Z. Li, Y. Xiao, and W. Liu, On the spin separation of algebraic two-component relativistic Hamiltonians, *J. Chem. Phys.*, 2012, **137**, 154114.

84 L. Cheng and J. Gauss, Analytic energy gradients for the spin-free exact two-component theory using an exact block diagonalization for the one-electron Dirac Hamiltonian, *J. Chem. Phys.*, 2011, **135**, 084114.

85 A. J. Cohen, P. Mori-Sánchez, and W. Yang, Development of exchange-correlation functionals with minimal many-electron self-interaction error, *J. Chem. Phys.*, 2007, **126**, 191109:1–5.

86 M. A. Ambroise and F. Jensen, Probing basis set requirements for calculating core ionization and core excitation spectroscopy by the Δ self-consistent-field approach, *J. Chem. Theory Comput.*, 2019, **15**, 325–337.

87 F. Jensen, Unifying general and segmented contracted basis sets. Segmented polarization consistent basis sets, *J. Chem. Theory Comput.*, 2014, **10**, 1074–1085.

88 D. E. Woon and T. H. Dunning Jr., Gaussian basis sets for use in correlated molecular calculations. IV. Calculation of static electrical response properties, *J. Chem. Phys.*, 1994, **100**, 2975–2988.

89 V. Barone and M. Cossi, Quantum calculation of molecular energies and energy gradients in solution by a conductor solvent model, *J. Phys. Chem. A*, 1998, **102**, 1995–2001.

90 T. N. Truong and E. V. Stefanovich, Analytical first and second energy derivatives of the generalized conductorlike screening model for free energy of solvation, *J. Chem. Phys.*, 1995, **103**, 3709–3717.

91 J. M. Herbert, Dielectric continuum methods for quantum chemistry, *WIREs Comput. Mol. Sci.*, 2021, **11**, e1519:1–73.